

## A study on the development of photoelastic experimental hybrid method for colour isochromatics ( I )<sup>†</sup>

Jai-sug Hawong<sup>1,\*</sup>, Jeong-hwan Nam<sup>1</sup>, Kyo-Hyoung Kim<sup>1</sup>, O-sung Kwon<sup>2</sup>, Gun Kwon<sup>2</sup> and Sung-han Park<sup>3</sup>

<sup>1</sup>Department of Mechanical Engineering, Yeungnam University, Gyeongsan, 712-749, Korea

<sup>2</sup>Graduate School of Mechanical Engineering, Yeungnam University, Gyeongsan, 712-749, Korea

<sup>3</sup>Agency for Defense Development, Daejeon, 305-152, Korea

(Manuscript Received October 9, 2009; Revised January 6, 2010; Accepted February 27, 2010)

### Abstract

Isochromatics obtained from photoelastic experiment shows the stress distributions of the full field of a structure under load. Therefore, stress distributions of the structure can be read at a glance through isochromatics. Many experimental data can be obtained from isochromatics which are then used in various photoelastic experimental hybrid methods for stress analysis. Monochromatic light has however, until now been used in the photoelastic experimental hybrid method to produce black and white isochromatics. The use of black and white isochromatics in photoelastic experimental hybrid method for black and white isochromatics requires high fringe orders in order to obtain sufficient experimental data for photoelastic hybrid techniques. Accordingly, this paper develops the photoelastic experimental hybrid method for color isochromatics in which a fringe order of 1 is enough to gather the experimental data of the photoelastic experimental hybrid method. The method was applied to validate stress concentration problems. Experimental results from this study indicated that the photoelastic experimental hybrid method for color isochromatics is more precise than the photoelastic experimental hybrid method for black and white isochromatics. The use of few fringe orders in photoelastic experimental hybrid method for color isochromatics can offer significant advantages in stress analysis of real components using reflective-type photoelastic experimental method.

**Keywords:** Photoelastic experimental hybrid method for white and black isochromatics; Photoelastic experimental hybrid method for color isochromatics; White and black isochromatics; Color isochromatics; Monochromatic light; White light; Stress concentration factor

### 1. Introduction

A theoretical method and an experimental method are used to analyze the stresses of structures under load. The theoretical method includes a pure analytical method and a numerical method. The experimental method includes the strain gage method [1, 2], moiré method [3-5], photoelastic experimental method [7-9], fatigue [10, 11], SPATE [12, 13], J-integral [14, 15], etc.

Among them, the photoelastic experimental method (the full field method) has been used in a variety of ways.

A 2-dimensional photoelastic experimental method [16] and a 3-dimensional photoelastic experimental method [17, 18] exist.

Although the 2-dimensional photoelastic experimental method has been studied extensively, the 3-dimensional photoelastic experimental method has yet to be studied to such a

degree.

The transparent-type photoelastic method and the reflective-type photoelastic experimental method [19-22] have been applied to study 2-dimensional photoelastic experiment. However, the reflective-type dynamic photoelastic experimental method in the 2-dimensional photoelastic experiment has not been studied.

In the future, we will study this field. The difference between two principal stresses ( $\sigma_1$  and  $\sigma_2$ ) is represented by fringe orders in the photoelastic method. Therefore, separating the two principal stresses in the photoelastic method is important. The shear difference method [23], interferometer method [24], electrical-analogy method [25] and oblique incidence method [26] can be used to separate the two principal stresses in the photoelastic experiment. But in these methods, many problems have to be solved with precision and a lot of work has to be done to process experimental data. To overcome these difficulties, there have been many studies on the photoelastic experimental hybrid method, which is used to study the internal stress of a model or structures under arbitrary load [27-35].

<sup>†</sup>This paper was recommended for publication in revised form by Associate Editor Tae Hee Lee

\*Corresponding author. Tel.: +82 53 810 2445, Fax: +82 53 810 4627  
E-mail address: jshawong@ynu.ac.kr

© KSME & Springer 2010

Until now, fringe orders greater than 4 are needed to produce accurate results using the photoelastic experimental hybrid method in photoelastic experiment. However, in the reflective-type photoelastic experiment applied to real structures, fringe orders less than 4 are produced. Therefore, a photoelastic experimental hybrid method that can be used to analyze the stresses of a model producing fringe orders of less than 4 needs to be developed.

This research develops the photoelastic experimental hybrid method for color isochromatics for fringe orders of less than 4.

## 2. Basic theory

### 2.1 Complex function representation of stresses

Stress components are given by Eq. (1) using the Airy stress function [36] with Muskhelishvili's complex function [37].

$$\begin{aligned}\sigma_x &= \operatorname{Re}\left\{2\phi'(z) - [\bar{z}\phi''(z) + \psi'(z)]\right\} \\ \sigma_y &= \operatorname{Re}\left\{2\phi'(z) + [\bar{z}\phi''(z) + \psi'(z)]\right\} \\ \tau_{xy} &= \operatorname{Im}\{\bar{z}\phi''(z) + \psi'(z)\}\end{aligned}\quad (1)$$

As shown in Eq. (1), once the stress functions  $\phi(z)$  and  $\psi(z)$  are determined, stress components ( $\sigma_x$ ,  $\sigma_y$  and  $\tau_{xy}$ ) can be determined. Therefore, the main problem becomes the determination of  $\phi(z)$  and  $\psi(z)$  in the stress analysis. This research develops the method that can provide the stress functions  $\phi(z)$  and  $\psi(z)$  using the photoelastic experimental method. Eq. (2) is a conformal mapping function.

$$z = w(\zeta) \quad (2)$$

Substituting Eq. (2) into (1) and using the traction-free condition on a free surface, the relative equation between stress functions  $\phi(z)$  and  $\psi(z)$  is obtained as Eq. (3) [38].

$$\psi(\zeta) = -\frac{\bar{w}(\zeta)}{w'(\zeta)} \phi'(\zeta) - \bar{\phi}(\zeta) \quad (3)$$

Instead of obtaining two stress functions,  $\phi(z)$  and  $\psi(z)$ , as in the conventional stress analysis, we obtain  $\phi(\zeta)$  satisfying the boundary conditions.

Using Eq. (3),  $\psi(\zeta)$  is obtained. Stress functions  $\phi(\zeta)$  and  $\psi(\zeta)$  can be transformed into  $\phi(z)$  and  $\psi(z)$  using the conformal mapping function. Substituting stress functions  $\phi(z)$  and  $\psi(z)$  into Eq. (1), stress components corresponding to the problem conditions are obtained.

What can be found by another method. Because  $\phi(\zeta)$  is an analytic stress function,  $\phi(\zeta)$  can be represented as a power series, as shown in Eq. (4).

$$\phi(\zeta) = \sum_{n=0}^N C_n (\zeta - \zeta_0)^n = \sum_{n=0}^N (a_n + ib_n)(\zeta - \zeta_0)^n \quad (4)$$

Complex coefficient  $C_n$  can be determined by using experimental data and a numerical method. Therefore, Eq. (4) is

determined.

Substituting Eq. (4) into Eq. (3) and using Eq. (3) with Eq. (4), Eqs. (2) and (1), stress components  $\sigma_x$ ,  $\sigma_y$  and  $\tau_{xy}$  are determined

$$\begin{aligned}\sigma_x &= \sum_{n=1}^N \operatorname{Re}\{C_n[2f(n,\zeta) - g(n,\zeta)] + \bar{C}_n f(n,\zeta)\} \\ \sigma_y &= \sum_{n=1}^N \operatorname{Re}\{C_n[2f(n,\zeta) + g(n,\zeta)] - \bar{C}_n f(n,\zeta)\} \\ \tau_{xy} &= \sum_{n=1}^N \operatorname{Im}\{C_n g(n,\zeta) - \bar{C}_n f(n,\zeta)\}\end{aligned}\quad (5)$$

Eq. (5) are stress components determined from the above procedure.

Eq. (6) presents  $f(n,\zeta)$  and  $g(n,\zeta)$  of Eq. (5)

$$f(n,\zeta) \equiv \frac{n(\zeta - \zeta_0)^{n-1}}{\omega'(\zeta)} \quad (6a)$$

$$\begin{aligned}g(n,\zeta) &\equiv \left[ \frac{\bar{\omega}(\bar{\zeta}) - \bar{\omega}(\zeta)}{\omega'(\zeta)^2} \right] n(n-1)(\zeta - \zeta_0)^{n-2} \\ &\quad - \left[ \frac{\bar{\omega}(\bar{\zeta}) - \bar{\omega}(\zeta)}{\omega'(\zeta)^3} \omega''(\zeta) + \frac{\bar{\omega}(\bar{\zeta})}{\omega'(\zeta)^2} \right] n(\zeta - \zeta_0)^{n-1}\end{aligned}\quad (6b)$$

Substituting the stress components obtained from the above procedures into the stress optic law, that is, Eq. (7) [39], Eq. (8) is determined.

$$(\sigma_1 - \sigma_2)^2 = (\sigma_x - \sigma_y)^2 + (2\tau_{xy})^2 = \left( \frac{f \cdot N_f}{t} \right)^2 \quad (7)$$

$$\begin{aligned}\left( \frac{f \cdot N_f}{t} \right)^2 &= \left\{ \sum_{n=1}^N a_n \operatorname{Re}[2f(n,\zeta) - 2g(n,\zeta)] \right. \\ &\quad + \sum_{n=1}^N b_n \operatorname{Im}[2f(n,\zeta) + 2g(n,\zeta)] \Big\}^2 \\ &\quad + \left\{ \sum_{n=1}^N a_n \operatorname{Im}[2g(n,\zeta) - 2f(n,\zeta)] \right. \\ &\quad + \sum_{n=1}^N b_n \operatorname{Re}[2f(n,\zeta) + 2g(n,\zeta)] \Big\}^2\end{aligned}\quad (8)$$

$f(n,\zeta)$  and  $g(n,\zeta)$  are functions of the position coordinates.

Position coordinates are determined using the inverse mapping function ( $\zeta = \omega^{-1}(z)$ ) when physical coordinates are known. Therefore Eq. (8) is a function of only  $a_n$  and  $b_n$ , and  $a_n$  and  $b_n$  are determined by using the nonlinear least square method.

Substituting the determined  $a_n$  and  $b_n$  into Eq. (4) and using Eqs. (2), (3) and (4) with the determined  $a_n$  and  $b_n$ , stress components [Eq. (1)] are determined. These procedures comprise the photoelastic experimental hybrid method.

## 2.2 Photoelastic experimental hybrid method for a circular hole

Eq. (9) is a conformal mapping function in the vicinity of a circular hole.

$$z = \omega(\zeta) = i\rho e^{-i\zeta} + z_1 = x + iy = re^{i\theta} + z_1 \quad (9a)$$

$$\frac{r}{\rho} e^{i\theta} = ie^{-i\zeta} = e^{i(\frac{\pi}{2}-\zeta)} \quad (9b)$$

$\omega'(\zeta)$ ,  $\omega(\zeta)$ ,  $\zeta - \zeta_0$  and  $\omega(\zeta)$  are determined using Eq. (9). Substituting the determined  $\omega'(\zeta)$ ,  $\omega(\zeta)$ ,  $\zeta - \zeta_0$  and  $\omega(\zeta)$  into Eq. (6),  $f(n, r, \theta)$  and  $g(n, r, \theta)$  for a circular hole are determined as shown in Eqs. (10a) and (10b), respectively.

$$f(n, r, \theta) = \frac{1}{r} e^{i(\frac{\pi}{2}-\theta)} n \left\{ \theta_0 - \theta + i \ln\left(\frac{r}{\rho}\right) \right\}^{n-1} \quad (10a)$$

$$g(n, r, \theta) = \frac{1}{r} \left( \frac{\rho^2}{r^2} - 1 \right) e^{-i3\theta} n(n-1) \left\{ \theta_0 - \theta + i \ln\left(\frac{r}{\rho}\right) \right\}^{n-2} + \frac{1}{r} \left( 2 \frac{\rho^2}{r^2} - 1 \right) e^{i(\frac{\pi}{2}-3\theta)} n \left\{ \theta_0 - \theta + i \ln\left(\frac{r}{\rho}\right) \right\}^{n-1} \quad (10b)$$

Substituting Eqs. (10a) and (10b) into Eq. (5) instead of  $f(n, \xi)$  and  $g(n, \xi)$ , stress components are determined as Eq. (11). Substituting Eq. (11) for (7), Eq. (12) is determined.

$$\begin{aligned} \sigma_x(r, \theta) &= \sum_{n=1}^N \operatorname{Re} \left\{ C_n [2f(n, r, \theta) - g(n, r, \theta)] + \overline{C_n} f(n, r, \theta) \right\} \\ \sigma_y(r, \theta) &= \sum_{n=1}^N \operatorname{Re} \left\{ C_n [2f(n, r, \theta) + g(n, r, \theta)] - \overline{C_n} f(n, r, \theta) \right\} \\ \tau_{xy}(r, \theta) &= \sum_{n=1}^N \operatorname{Im} \left\{ C_n g(n, r, \theta) - \overline{C_n} f(n, r, \theta) \right\} \end{aligned} \quad (11)$$

Eq. (12) is the stress optic law, which substitutes the position vector of the z-plane with the circular diameter  $\rho$ .

$$\begin{aligned} &= \left\{ \sum_{n=1}^N a_n \operatorname{Re} [2f(n, r, \theta) - 2g(n, r, \theta)] \right. \\ &\quad \left. + \sum_{n=1}^N b_n \operatorname{Im} [2f(n, r, \theta) + 2g(n, r, \theta)] \right\}^2 \\ &\quad + \left\{ \sum_{n=1}^N a_n \operatorname{Im} [2g(n, r, \theta) - 2f(n, r, \theta)] \right. \\ &\quad \left. + \sum_{n=1}^N b_n \operatorname{Re} [2f(n, r, \theta) + 2g(n, r, \theta)] \right\}^2 \\ &\quad - \left( \frac{f \cdot N_f}{t} \right)^2 = 0 \end{aligned} \quad (12)$$

Applying the numerical method to Eq. (12), in which the

Table 1. Color isochromatic fringe characteristics.

| Color   | Fringe order (N) |
|---|------------------|
| Black   | 0                |
| Gray  | 0.08             |
| White   | 0.45             |
| Pale yellow                                   | 0.6              |
| Orange  | 0.8              |
| Dull red                                      | 0.9              |
| Purple (tint of passage no. 1)                | 1                |
| Deep blue                                     | 1.08             |
| Blue-green                                    | 1.22             |
| Green-yellow                                  | 1.39             |
| Orange  | 1.63             |
| Rose red                                      | 1.82             |
| Purple (tint of passage no. 2)                | 2                |
| Green   | 2.35             |
| Green-yellow                                  | 2.5              |
| Red   | 2.65             |
| Red/green transition (tint of passage no. 3)  | 3                |
| Green   | 3.1              |
| Pink  | 3.65             |
| Pink/green transition (tint of passage no. 4) | 4                |
| Green   | 4.15             |

fringe orders and the position vector corresponding to the fringe orders are substituted, coefficients  $a_n$  and  $b_n$  of stress function are determined. Substituting the determined  $a_n$  and  $b_n$  for  $\phi(\zeta)$  and using Eqs. (2) and (3), stress functions  $\phi(z)$  and  $\psi(z)$  are determined. Substituting the determined  $\phi(z)$  and  $\psi(z)$  into Eq. (1), the stress components in the vicinity of the circular hole in the plate under arbitrary load are determined. These procedures comprise the photoelastic experimental hybrid method. Until now, the needed experimental data measured from the black and white isochromatics have been applied to Eq. (12). The procedures obtaining  $(\sigma_x, \sigma_y, \tau_{xy})$  using black and white isochromatics comprise the photoelastic experimental hybrid method for white and black isochromatics.

In this paper, the needed experimental data measured from color isochromatics are applied to the modified Eq. (12) and using the procedures explained in the previous page, stress components are determined. These procedures comprise the photoelastic experimental hybrid method for color isochromatics.

## 3. Experiment and experimental method

Both the transparent-type photoelastic experimental method and the reflective-type experimental method have been utilized in stress analysis. In general, the fringe orders of isochromatics are high in the transparent-type photoelastic experiment and very low in the reflective-type photoelastic experiment.

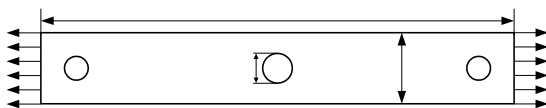


Fig. 1. Specimens of transmission type photoelastic experiment.

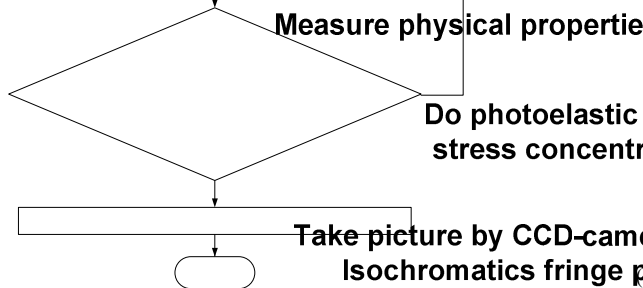
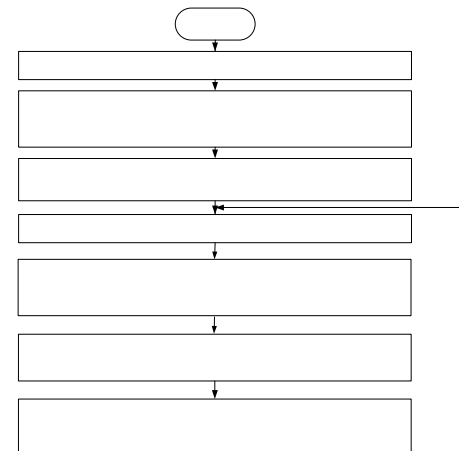


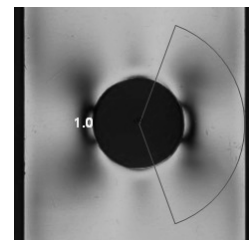
Fig. 2. Flow chart of photoelastic experimental hybrid method for color isochromatics.

To develop the photoelastic experimental hybrid method for color isochromatics, the transparent-type photoelastic experimental device with a white light source was used in this research. Using a white light source, color isochromatics were produced. Table 1 indicates the relationship between fringe order ( $N$ ) and color [40].

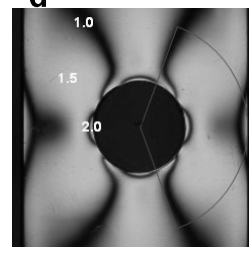
Color fringe orders are repeated according to the same sequence as shown in Table 1, but the tones of color isochromatics become more and more indistinct. Therefore, when fringe orders are greater than 4, the color isochromatic is vague. As shown in Table 1, when the fringe orders are greater than 4 we cannot distinguish fringe orders in detail.

To verify the effectiveness of the photoelastic experimental hybrid method for the color isochromatics developed in this research, the transparent-type photoelastic experiment was carried out on the rectangular specimen with a circular hole under uniform tension. Fig. 1 shows the specimen size used in this research. The height ( $h$ ), the diameter ( $d$ ), the width ( $w$ ) and the thickness ( $t$ ) of the finite rectangular plate are, respectively,  $h=200\text{mm}$ ,  $d=12\text{mm}$ ,  $w=30\text{mm}$ , and  $t=3\text{mm}$ .

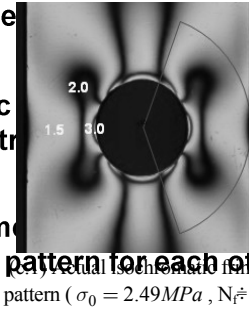
The numerical method used in the photoelastic experimental hybrid method for color isochromatics is the Hook and Jeeve's numerical method [41]. Fig. 2 shows the flow chart of



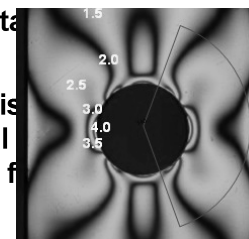
(a.1) Actual isochromatic fringe pattern ( $\sigma_0 = 0.98\text{MPa}$ ,  $N_f \approx 1$ )



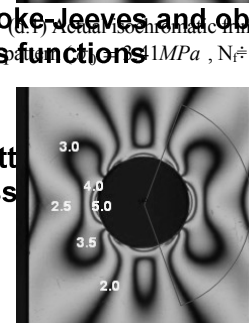
(a.2) Plotted isochromatic fringe pattern ( $\sigma_0 = 0.98\text{MPa}$ ,  $N_f \approx 1$ )



(b.1) Actual isochromatic fringe pattern ( $\sigma_0 = 1.78\text{MPa}$ ,  $N_f \approx 2$ )

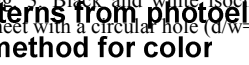


(b.2) Plotted isochromatic fringe pattern ( $\sigma_0 = 1.78\text{MPa}$ ,  $N_f \approx 2$ )



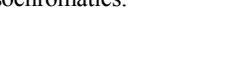
(c.1) Actual isochromatic fringe pattern ( $\sigma_0 = 2.49\text{MPa}$ ,  $N_f \approx 3$ )

(c.2) Plotted isochromatic fringe pattern ( $\sigma_0 = 2.49\text{MPa}$ ,  $N_f \approx 3$ )



(d.1) Actual isochromatic fringe pattern ( $\sigma_0 = 3.41\text{MPa}$ ,  $N_f \approx 4$ )

(d.2) Plotted isochromatic fringe pattern ( $\sigma_0 = 3.41\text{MPa}$ ,  $N_f \approx 4$ )



(e.1) Actual isochromatic fringe pattern ( $\sigma_0 = 4.06\text{MPa}$ ,  $N_f \approx 5$ )

(e.2) Plotted isochromatic fringe pattern ( $\sigma_0 = 4.06\text{MPa}$ ,  $N_f \approx 5$ )



(f.1) Actual isochromatic fringe pattern ( $\sigma_0 = 4.06\text{MPa}$ ,  $N_f \approx 5$ )

(f.2) Plotted isochromatic fringe pattern ( $\sigma_0 = 4.06\text{MPa}$ ,  $N_f \approx 5$ )



(g.1) Actual isochromatic fringe pattern ( $\sigma_0 = 4.06\text{MPa}$ ,  $N_f \approx 5$ )

(g.2) Plotted isochromatic fringe pattern ( $\sigma_0 = 4.06\text{MPa}$ ,  $N_f \approx 5$ )



(h.1) Actual isochromatic fringe pattern ( $\sigma_0 = 4.06\text{MPa}$ ,  $N_f \approx 5$ )

(h.2) Plotted isochromatic fringe pattern ( $\sigma_0 = 4.06\text{MPa}$ ,  $N_f \approx 5$ )



(i.1) Actual isochromatic fringe pattern ( $\sigma_0 = 4.06\text{MPa}$ ,  $N_f \approx 5$ )

(i.2) Plotted isochromatic fringe pattern ( $\sigma_0 = 4.06\text{MPa}$ ,  $N_f \approx 5$ )



(j.1) Actual isochromatic fringe pattern ( $\sigma_0 = 4.06\text{MPa}$ ,  $N_f \approx 5$ )

(j.2) Plotted isochromatic fringe pattern ( $\sigma_0 = 4.06\text{MPa}$ ,  $N_f \approx 5$ )



(k.1) Actual isochromatic fringe pattern ( $\sigma_0 = 4.06\text{MPa}$ ,  $N_f \approx 5$ )

(k.2) Plotted isochromatic fringe pattern ( $\sigma_0 = 4.06\text{MPa}$ ,  $N_f \approx 5$ )



(l.1) Actual isochromatic fringe pattern ( $\sigma_0 = 4.06\text{MPa}$ ,  $N_f \approx 5$ )

(l.2) Plotted isochromatic fringe pattern ( $\sigma_0 = 4.06\text{MPa}$ ,  $N_f \approx 5$ )



(m.1) Actual isochromatic fringe pattern ( $\sigma_0 = 4.06\text{MPa}$ ,  $N_f \approx 5$ )

(m.2) Plotted isochromatic fringe pattern ( $\sigma_0 = 4.06\text{MPa}$ ,  $N_f \approx 5$ )



(n.1) Actual isochromatic fringe pattern ( $\sigma_0 = 4.06\text{MPa}$ ,  $N_f \approx 5$ )

(n.2) Plotted isochromatic fringe pattern ( $\sigma_0 = 4.06\text{MPa}$ ,  $N_f \approx 5$ )



(o.1) Actual isochromatic fringe pattern ( $\sigma_0 = 4.06\text{MPa}$ ,  $N_f \approx 5$ )

(o.2) Plotted isochromatic fringe pattern ( $\sigma_0 = 4.06\text{MPa}$ ,  $N_f \approx 5$ )



(p.1) Actual isochromatic fringe pattern ( $\sigma_0 = 4.06\text{MPa}$ ,  $N_f \approx 5$ )

(p.2) Plotted isochromatic fringe pattern ( $\sigma_0 = 4.06\text{MPa}$ ,  $N_f \approx 5$ )



(q.1) Actual isochromatic fringe pattern ( $\sigma_0 = 4.06\text{MPa}$ ,  $N_f \approx 5$ )

(q.2) Plotted isochromatic fringe pattern ( $\sigma_0 = 4.06\text{MPa}$ ,  $N_f \approx 5$ )



(r.1) Actual isochromatic fringe pattern ( $\sigma_0 = 4.06\text{MPa}$ ,  $N_f \approx 5$ )

(r.2) Plotted isochromatic fringe pattern ( $\sigma_0 = 4.06\text{MPa}$ ,  $N_f \approx 5$ )



(s.1) Actual isochromatic fringe pattern ( $\sigma_0 = 4.06\text{MPa}$ ,  $N_f \approx 5$ )

(s.2) Plotted isochromatic fringe pattern ( $\sigma_0 = 4.06\text{MPa}$ ,  $N_f \approx 5$ )



(t.1) Actual isochromatic fringe pattern ( $\sigma_0 = 4.06\text{MPa}$ ,  $N_f \approx 5$ )

(t.2) Plotted isochromatic fringe pattern ( $\sigma_0 = 4.06\text{MPa}$ ,  $N_f \approx 5$ )



(u.1) Actual isochromatic fringe pattern ( $\sigma_0 = 4.06\text{MPa}$ ,  $N_f \approx 5$ )

(u.2) Plotted isochromatic fringe pattern ( $\sigma_0 = 4.06\text{MPa}$ ,  $N_f \approx 5$ )



(v.1) Actual isochromatic fringe pattern ( $\sigma_0 = 4.06\text{MPa}$ ,  $N_f \approx 5$ )

(v.2) Plotted isochromatic fringe pattern ( $\sigma_0 = 4.06\text{MPa}$ ,  $N_f \approx 5$ )



(w.1) Actual isochromatic fringe pattern ( $\sigma_0 = 4.06\text{MPa}$ ,  $N_f \approx 5$ )

(w.2) Plotted isochromatic fringe pattern ( $\sigma_0 = 4.06\text{MPa}$ ,  $N_f \approx 5$ )



(x.1) Actual isochromatic fringe pattern ( $\sigma_0 = 4.06\text{MPa}$ ,  $N_f \approx 5$ )

(x.2) Plotted isochromatic fringe pattern ( $\sigma_0 = 4.06\text{MPa}$ ,  $N_f \approx 5$ )



(y.1) Actual isochromatic fringe pattern ( $\sigma_0 = 4.06\text{MPa}$ ,  $N_f \approx 5$ )

(y.2) Plotted isochromatic fringe pattern ( $\sigma_0 = 4.06\text{MPa}$ ,  $N_f \approx 5$ )



(z.1) Actual isochromatic fringe pattern ( $\sigma_0 = 4.06\text{MPa}$ ,  $N_f \approx 5$ )

(z.2) Plotted isochromatic fringe pattern ( $\sigma_0 = 4.06\text{MPa}$ ,  $N_f \approx 5$ )



(aa.1) Actual isochromatic fringe pattern ( $\sigma_0 = 4.06\text{MPa}$ ,  $N_f \approx 5$ )

(aa.2) Plotted isochromatic fringe pattern ( $\sigma_0 = 4.06\text{MPa}$ ,  $N_f \approx 5$ )



(ab.1) Actual isochromatic fringe pattern ( $\sigma_0 = 4.06\text{MPa}$ ,  $N_f \approx 5$ )

(ab.2) Plotted isochromatic fringe pattern ( $\sigma_0 = 4.06\text{MPa}$ ,  $N_f \approx 5$ )



(ac.1) Actual isochromatic fringe pattern ( $\sigma_0 = 4.06\text{MPa}$ ,  $N_f \approx 5$ )

(ac.2) Plotted isochromatic fringe pattern ( $\sigma_0 = 4.06\text{MPa}$ ,  $N_f \approx 5$ )



(ad.1) Actual isochromatic fringe pattern ( $\sigma_0 = 4.06\text{MPa}$ ,  $N_f \approx 5$ )

(ad.2) Plotted isochromatic fringe pattern ( $\sigma_0 = 4.06\text{MPa}$ ,  $N_f \approx 5$ )



(ae.1) Actual isochromatic fringe pattern ( $\sigma_0 = 4.06\text{MPa}$ ,  $N_f \approx 5$ )

(ae.2) Plotted isochromatic fringe pattern ( $\sigma_0 = 4.06\text{MPa}$ ,  $N_f \approx 5$ )



(af.1) Actual isochromatic fringe pattern ( $\sigma_0 = 4.06\text{MPa}$ ,  $N_f \approx 5$ )

(af.2) Plotted isochromatic fringe pattern ( $\sigma_0 = 4.06\text{MPa}$ ,  $N_f \approx 5$ )



(ag.1) Actual isochromatic fringe pattern ( $\sigma_0 = 4.06\text{MPa}$ ,  $N_f \approx 5$ )

(ag.2) Plotted isochromatic fringe pattern ( $\sigma_0 = 4.06\text{MPa}$ ,  $N_f \approx 5$ )



(ah.1) Actual isochromatic fringe pattern ( $\sigma_0 = 4.06\text{MPa}$ ,  $N_f \approx 5$ )

(ah.2) Plotted isochromatic fringe pattern ( $\sigma_0 = 4.06\text{MPa}$ ,  $N_f \approx 5$ )



(ai.1) Actual isochromatic fringe pattern ( $\sigma_0 = 4.06\text{MPa}$ ,  $N_f \approx 5$ )

(ai.2) Plotted isochromatic fringe pattern ( $\sigma_0 = 4.06\text{MPa}$ ,  $N_f \approx 5$ )



(aj.1) Actual isochromatic fringe pattern ( $\sigma_0 = 4.06\text{MPa}$ ,  $N_f \approx 5$ )

(aj.2) Plotted isochromatic fringe pattern ( $\sigma_0 = 4.06\text{MPa}$ ,  $N_f \approx 5$ )



(ak.1) Actual isochromatic fringe pattern ( $\sigma_0 = 4.06\text{MPa}$ ,  $N_f \approx 5$ )

(ak.2) Plotted isochromatic fringe pattern ( $\sigma_0 = 4.06\text{MPa}$ ,  $N_f \approx 5$ )



(al.1) Actual isochromatic fringe pattern ( $\sigma_0 = 4.06\text{MPa}$ ,  $N_f \approx 5$ )

(al.2) Plotted isochromatic fringe pattern ( $\sigma_0 = 4.06\text{MPa}$ ,  $N_f \approx 5$ )



(am.1) Actual isochromatic fringe pattern ( $\sigma_0 = 4.06\text{MPa}$ ,  $N_f \approx 5$ )

(am.2) Plotted isochromatic fringe pattern ( $\sigma_0 = 4.06\text{MPa}$ ,  $N_f \approx 5$ )



(an.1) Actual isochromatic fringe pattern ( $\sigma_0 = 4.06\text{MPa}$ ,  $N_f \approx 5$ )

(an.2) Plotted isochromatic fringe pattern ( $\sigma_0 = 4.06\text{MPa}$ ,  $N_f \approx 5$ )



(ao.1) Actual isochromatic fringe pattern ( $\sigma_0 = 4.06\text{MPa}$ ,  $N_f \approx 5$ )

(ao.2) Plotted isochromatic fringe pattern ( $\sigma_0 = 4.06\text{MPa}$ ,  $N_f \approx 5$ )



(ap.1) Actual isochromatic fringe pattern ( $\sigma_0 = 4.06\text{MPa}$ ,  $N_f \approx 5$ )

(ap.2) Plotted isochromatic fringe pattern ( $\sigma_0 = 4.06\text{MPa}$ ,  $N_f \approx 5$ )



(aq.1) Actual isochromatic fringe pattern ( $\sigma_0 = 4.06\text{MPa}$ ,  $N_f \approx 5$ )

(aq.2) Plotted isochromatic fringe pattern ( $\sigma_0 = 4.06\text{MPa}$ ,  $N_f \approx 5$ )



(ar.1) Actual isochromatic fringe pattern ( $\sigma_0 = 4.06\text{MPa}$ ,  $N_f \approx 5$ )

(ar.2) Plotted isochromatic fringe pattern ( $\sigma_0 = 4.06\text{MPa}$ ,  $N_f \approx 5$ )



(as.1) Actual isochromatic fringe pattern ( $\sigma_0 = 4.06\text{MPa}$ ,  $N_f \approx 5$ )

(as.2) Plotted isochromatic fringe pattern ( $\sigma_0 = 4.06\text{MPa}$ ,  $N_f \approx 5$ )



(at.1) Actual isochromatic fringe pattern ( $\sigma_0 = 4.06\text{MPa}$ ,  $N_f \approx 5$ )

(at.2) Plotted isochromatic fringe pattern ( $\sigma_0 = 4.06\text{MPa}$ ,  $N_f \approx 5$ )



(au.1) Actual isochromatic fringe pattern ( $\sigma_0 = 4.06\text{MPa}$ ,  $N_f \approx 5$ )

(au.2) Plotted isochromatic fringe pattern ( $\sigma_0 = 4.06\text{MPa}$ ,  $N_f \approx 5$ )



(av.1) Actual isochromatic fringe pattern ( $\sigma_0 = 4.06\text{MPa}$ ,  $N_f \approx 5$ )

(av.2) Plotted isochromatic fringe pattern ( $\sigma_0 = 4.06\text{MPa}$ ,  $N_f \approx 5$ )



(aw.1) Actual isochromatic fringe pattern ( $\sigma_0 = 4.06\text{MPa}$ ,  $N_f \approx 5$ )

(aw.2) Plotted isochromatic fringe pattern ( $\sigma_0 =$

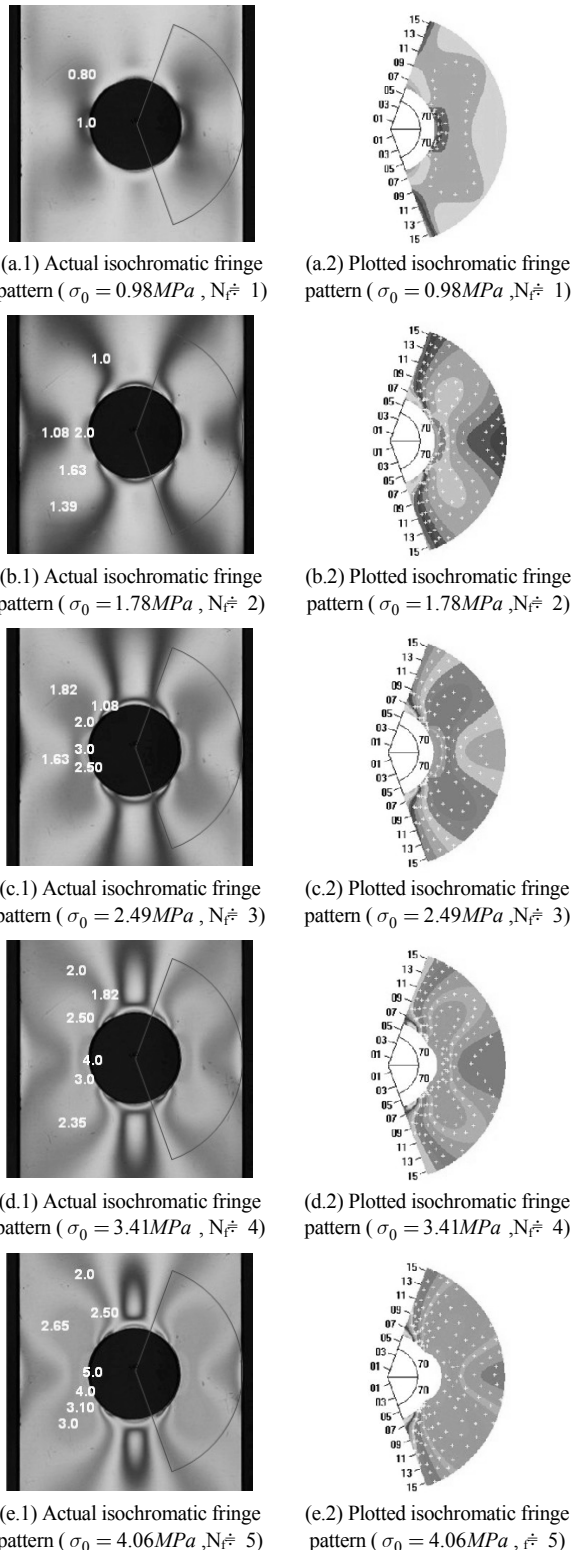


Fig. 4. Color isochromatic fringe patterns for rectangular sheet with circular hole ( $d/w=0.39$ ).

#### 4. Experimental results and discussions

(a), (b), (c), (d) and (e) in Fig. 3 show the actual black and white fringe patterns (left side) and plotted isochromatic fringe

patterns (right side) of specimens with applied loads of 146.5N, 266.64N, 393.29N, 511.05N and 608.82N, and fringe orders of about 1, 2, 3, 4 and 5 respectively, with  $d/w$  of 0.39.

Fig. 4 shows the color isochromatic fringe patterns obtained from the same loading and geometrical conditions as those of Fig. 3.

Plotted isochromatic fringe patterns (right side) of Fig. 3 and Fig. 4 show, respectively, graphic fan-shaped isochromatics obtained from the conventional photoelastic experimental hybrid method for black and white isochromatics and the photoelastic experimental hybrid method for color isochromatics developed in this research.

The numbers on the fringes indicate fringe orders. The fan-shaped region is the region where experimental data is measured. “+” marks on the fringes of the plotted isochromatics in Fig. 3 and Fig. 4 indicate the positions from where experimental data were measured.

Experimental data were measured on the centerline of the white and black bands in the black and white isochromatics. All the “+” marks are located on the centerline of the white and black bands in Fig. 3. This means that the conventional photoelastic experimental hybrid method is valid.

On the other hand, experimental data were measured on the centerline of each fringe order in the color isochromatics.

Since all the “+” marks are located on the centerline of each fringe order in Fig. 4, it means that the experimental hybrid method for the color isochromatics is effective.

(a.1), (b.1), (c.1), (d.1) and (e.1) of Fig. 3 and Fig. 4 show black and white isochromatics and color isochromatics for fringe orders of about 1, 2, 3, 4, and 5, respectively.

(a.2), (b.2), (c.2), (d.2) and (e.2) of Fig. 3 and Fig. 4 show the graphic isochromatics obtained from the photoelastic experimental hybrid method for black and white isochromatics and photoelastic experimental hybrid method for color isochromatics when the fringe order is about 1, 2, 3, 4 and 5.

When the maximum fringe order is 1, the graphic isochromatics obtained from the photoelastic experimental hybrid method for black and white isochromatics is completely different from the actual isochromatics, but the graphic isochromatics obtained from the photoelastic experimental hybrid method for color isochromatics is very similar to the actual isochromatics. When the maximum fringe order is about 2, the graphic isochromatics obtained from the photoelastic experimental hybrid method for black and white isochromatics is different from the actual black and white isochromatics, but graphic isochromatics obtained from the photoelastic experimental hybrid method for color isochromatics is almost identical to the actual isochromatics.

When the maximum fringe order is about 3, the graphic isochromatics obtained from the photoelastic experimental hybrid method for black and white isochromatics is very similar to the actual black and white isochromatics, and the graphic isochromatics obtained from the photoelastic experimental hybrid method for color isochromatics is identical to the actual color isochromatics.

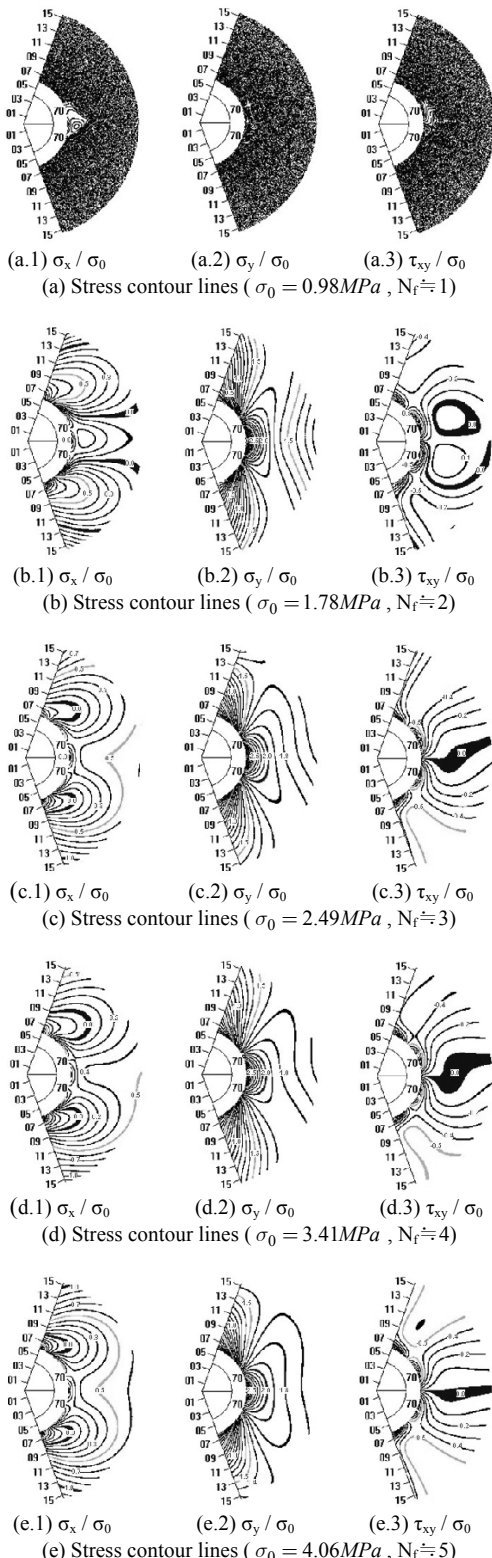


Fig. 5. Stress contour lines for rectangular sheet with circular hole ( $d/w=0.39$ ).

When the maximum fringe order is about 4, the graphic isochromatics obtained from the photoelastic experimental hybrid method for black and white isochromatics is very simi-

lar to the actual black and white isochromatics, and the graphic isochromatics obtained from the photoelastic experimental hybrid method for color isochromatics is identical to the actual color isochromatics.

When the maximum fringe order is 5, the graphic isochromatics obtained from the photoelastic experimental hybrid method for black and white isochromatics is almost identical to the actual black and white isochromatics, and the graphic isochromatics obtained from the photoelastic experimental hybrid method for color isochromatics is completely identical to the actual color isochromatics.

The photoelastic experimental hybrid method for black and white isochromatics can be accurately used when the maximum fringe order is greater than or equal to 4.

The photoelastic experimental hybrid method for color isochromatics can be effectively used when the maximum fringe order is greater than 1 or equal to 1.

Fig. 5 and Fig. 6 are, respectively, stress contours obtained from the photoelastic experimental hybrid method for black and white isochromatics and for color isochromatics.

Fig. 5 shows the stress contours obtained from the photoelastic experimental hybrid method for black and white isochromatics of Fig. 3.

As shown in Fig. 3(a.1), when the maximum fringe order is about 1, black and white isochromatics are very vague and the position of the fringe orders is not clear; therefore, the needed experimental data cannot be measured, and thus,  $\sigma_x/\sigma_0$ ,  $\sigma_y/\sigma_0$ ,  $\tau_{xy}/\sigma_0$  cannot be calculated. They are almost zero, as shown in Fig. 5(a.1).

When the maximum fringe order is greater than about 3 and 4, a similar pattern of stress distributions of the stress components ( $\sigma_x/\sigma_0$ ,  $\sigma_y/\sigma_0$ ,  $\tau_{xy}/\sigma_0$ ) are obtained.

When the maximum fringe order is 5, the stress distributions of the stress components from the photoelastic experimental hybrid method for black and white isochromatics are very similar to those from the photoelastic experimental hybrid method for color isochromatics.

Fig. 6 shows the stress contours of stress components obtained from the photoelastic experimental hybrid method for color isochromatics of Fig. 4.

When the maximum fringe order is about 1, stress components are obtained. When the maximum fringe order is about 2, more accurate stress components are obtained.

When the maximum fringe order is greater than or equal to about 3, similar distribution patterns of accurate stress components are obtained.

As shown in Fig. 3, Fig. 4, Fig. 5 and Fig. 6, the photoelastic experimental hybrid method for black and white isochromatics can be effectively used when the maximum fringe order is greater than or equal to 4.

The photoelastic experimental hybrid method for color isochromatics developed in this research can be effectively used when the maximum fringe order is greater than or equal to 1.

Table 2 gives the stress concentration factors  $\alpha_k$  obtained

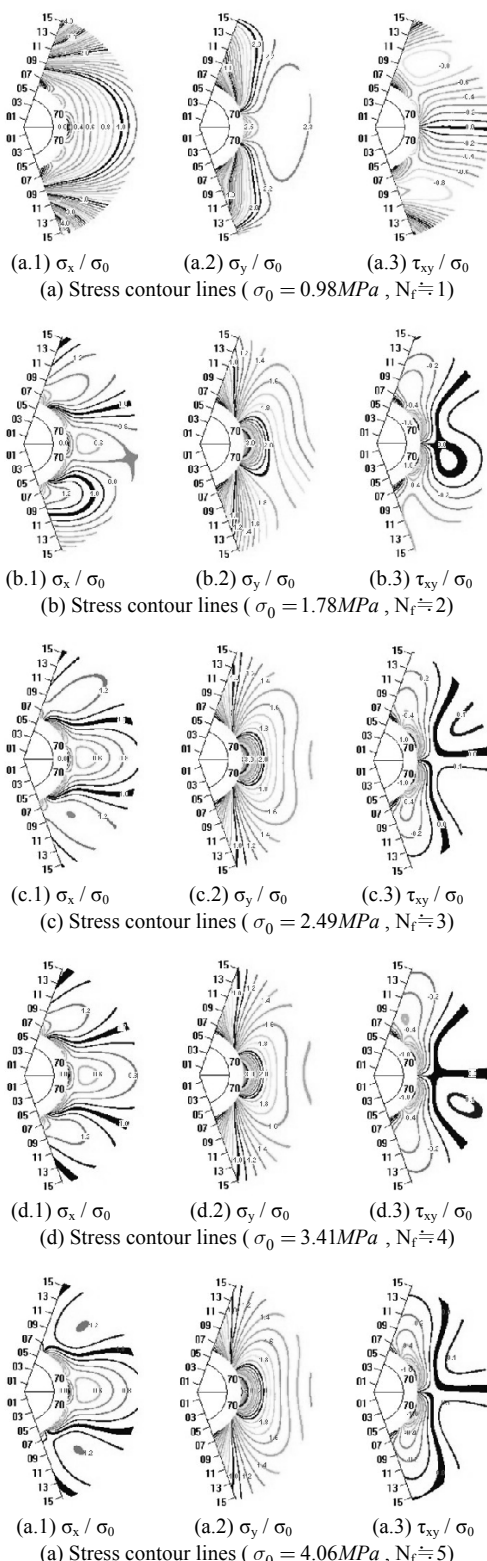


Fig. 6. Stress contour lines for rectangular sheet with circular hole ( $d/w=0.39$ ).

from the photoelastic experimental hybrid method for black and white isochromatics and for color isochromatics for a rectangular plate with a circular hole under uniform tension.

Table 2. Values of stress concentration factors  $\alpha_K$  for rectangular sheet with circular hole.

| $d/w$ | N | P(N)    | $\sigma_0$ | Stress Concentration Factor( $\alpha_K$ ) |           | Theo value<br>(41) |  |
|-------|---|---------|------------|---|-----------|--------------------|--|
|       |   |         |            | Black & White                             |           |                    |  |
|       |   |         |            | Exp. value                                | Error [%] |                    |  |
| 0.39  | 1 | 146.650 | 0.714      | 5.561                                     | 50.987    | 3.126 15.131       |  |
|       | 2 | 266.636 | 1.298      | 4.622                                     | 25.471    | 3.790 2.882        |  |
|       | 3 | 373.290 | 1.817      | 4.470                                     | 21.352    | 3.755 1.937        |  |
|       | 4 | 511.052 | 2.487      | 4.305                                     | 16.867    | 3.729 1.239        |  |
|       | 5 | 608.818 | 2.963      | 4.079                                     | 10.734    | 3.714 0.831        |  |

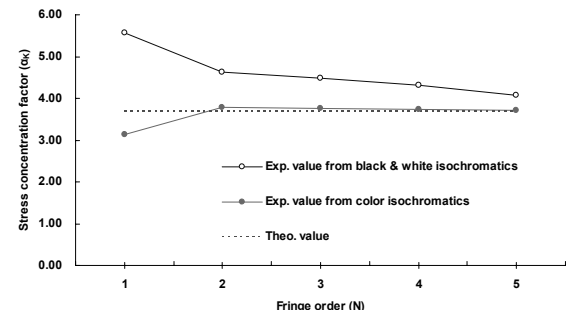


Fig. 7. Stress concentration factor  $\alpha_K$  with respect to fringe order for a rectangular sheet with a circular hole.

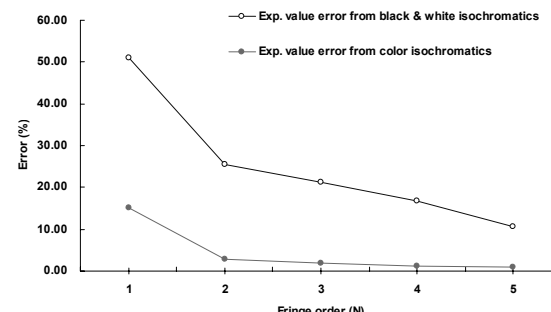


Fig. 8. Errors with respect to fringe order for rectangular sheet with circular hole.

$$\text{Error}(\%) = \frac{|\text{Theo.value} - \text{Exp.value}|}{\text{Theo.value}} \times 100$$

Fig. 7 and Fig. 8 respectively show stress concentration factors and errors with fringe orders.

As shown in Table 2, Fig. 7 and Fig. 8, when the maximum fringe order is 4, the error of experimental values from the photoelastic experimental hybrid method for black and white isochromatics is about 17%.

When the maximum fringe order is 5, the error from the photoelastic experimental hybrid method for black and white isochromatics is about 11%.

When the maximum fringe order is 2, the error from the photoelastic experimental hybrid method for color isochromatics is about 3%. When the maximum fringe order is 1, the errors from the photoelastic experimental hybrid method for

color isochromatics are about 15%.

The errors in the specific number of the fringe numbers in this paper universally resulted from the different geometries of mechanical elements.

As shown in Table 2, the photoelastic experimental hybrid method for black and white isochromatics can be effectively used in stress analysis when the maximum fringe orders are greater than or equal to about 4.

The photoelastic experimental hybrid method for color isochromatics can be effectively used in stress analysis when the maximum fringe order is greater than or equal to 1.

## 5. Conclusions

The following conclusions are obtained from previous experiments and experimental results.

1. A photoelastic experimental hybrid method for color isochromatics was developed and its validity was certified.
2. In stress analysis and separation of stress components using photoelastic technique, the photoelastic experimental hybrid method for black and white isochromatics can be effectively used when the maximum fringe order is greater than or equal to 4. However, when the maximum fringe order is greater than or equal to about 1, the photoelastic experimental hybrid method for color isochromatics can be effectively used.
3. When the maximum fringe orders are about 4 and about 5, the errors of experimental values obtained from the photoelastic experimental hybrid method for black and white isochromatics are about 17% and 11%, respectively. On the other hand, when maximum fringe orders are about 1 and about 2, the errors from photoelastic experimental hybrid color isochromatics are about 15% and about 3%, respectively, in stress concentration problems.

## References

- [1] J. W. Dally and R. J. Sanford, Strain Gage Methods for Measuring the Opening Mode Stress Intensity Factor,  $K_1$ , *Exp. Mech.*, 27 (4) (1987) 381-388.
- [2] J. R. Berger and J. W. Dally, An Overdeterministic Approach for Measuring  $K_1$  Using Strain Gages, *Exp. Mech.*, 28 (2) (1988) 142-145.
- [3] R. E. Rowlands, I. M. Daniel and J. B. Whiteside, Stress and Failure Analysis of a Glass-Epoxy Composite Plate with a Circular Hole, *Exp. Mech.*, (1973) 31-37.
- [4] D. Post, R. Czarnek and D. Joh, Shear Strains in a Graphite /peek Beam by Moire Interferometry with Carrier Fringes, *Exp. Mech.*, (1987) 246-249.
- [5] A. J. Durelli and V. J. Parks, *Moire Analysis of strain*, Prentice-Hall, Inc. Englewood Cliffs, New Jersey, (1970).
- [6] Dally J. W. and W. F. Riley, *Experimental Stress Analysis*, 2<sup>nd</sup> Edition, McGraw-Hill, Inc. (1978).
- [7] Kuske, A. and G. Robertson, *Photoelastic Stress Analysis*, John. Wiley & Sons, Inc. (1974).
- [8] R. J. Craig, M. J. Gutziwiwiller, R. H. Lee and E. O. Stitz, A Composite Three-Dimensional Photoelastic Method, *Exp. Mech.*, (1977) 433-438.
- [9] O. S. Lee and K. Y. Nam, Theoretical Photoelastic Stresses in Three Dimensional Body with Elastic Contact, KSME international Journal, 13 (4) (1999) 321-331.
- [10] J. Watanabe, T. Iwadate, Yo Tanaka, T. Yokoboro and K. Anodo, Fracture Toughness in the Tansition Region, *Engineering Fracture Mechanics*, 28 (1987) 589-600.
- [11] D. S. Mountain and J. M. B. Webber, Stress Pattern Analysis by Thermal Emmission (SPATE), *Proc. Soc. Pho-Opt., Inst. Engrs.*, 164 (1978) 189-196.
- [12] Y. M. Huang, H. Abdelmohsen, D. Lohr, Z. Feng, R. E. Rowlands and P. Stanley, Determination of Individual Stress Components from SPATE Isopachics only, *Proc. 6<sup>th</sup> Inter. Cong. On Exp. Mech.*, SEM, Portland, Oregon, (1988) 578-584.
- [13] J. R. Rice, P. C. Paris and J. G. Merkle, Some Futher Results of J-Integral Analysis and Estimates, ASTM STP 536, *American Society of Testing and Materials, Philadelphia*, (1973) 231-245.
- [14] C. F. Shih, Relationship between the J-integral and crack Opening Displacement for Stationary and Extending cracks. *Journal of the Mechanics and physics of solids*, 29 (1981) 305-326.
- [15] D. Drucker and R. Mindlin, Stress Analysis by Three-dimensional Photoelastic Methods, *J. Appl. Phys.*, 11 (1940) 724-732.
- [16] R. Hiltscher, Development of Lateral Extensometer Method in Two-Dimensional Photoelasticity. *Proc. Int. Sym. Illinois Institute of Technology*, Pergamon Press, (1963) 43.
- [17] D. C. Drucker and W. B. Woodward, Interpretation of Photoelastic Transmission Patterns for Three-dimensional Model, *J. Appl. Phys.*, 25 (4) (1954) 510-512.
- [18] F. Zandman, S. Redner and J. W. Dally, *Photoelastic Coatings*, The Iowa State University Press, Society for Experimental Stress Analysis. (1977).
- [19] R. Fleury and F. Zandman, 1954, Jauge d'Efforts Photoelastique, *Comptes Rendus*, Paris, (1559) 238.
- [20] K. Kawata, Analysis of Elastoplastic Behavior of Metals by Means of the Photoelastic Coating Method, *J. Sci. Res. Inst.*, Tokyo, 52 (1958) 17-40.
- [21] F. Zandman, Stress Analysis of a Guided Missile Tail Section with the Photoelastic Technique, *Proc. SESA*, 17 (2) (1960) 135-150.
- [22] M. H. L. Frocht, *Photoelasticity*, vol. 1, Chap. 8, John Wiley & Sons, Inc., New York, 1941.
- [23] D. Post, A New Photoelastic Interferometer Suitable for Static and Dynamic Measurements, *Proc. SESA*, X II (1) (1954) 191-202.
- [24] W. F. Stokey and W. F. Hughes, Tests of the Conducting Paper Analogy for Determining Isopachic Lines, *Proc. SESA*, X II (2) (1955) 77-82.
- [25] D. C. Drucker, Photoelastic Separation of Principal Stresses by Oblique Incidence, *J. Appl. Mech.*, 10 (3) (1943) A156-

A160.

- [26] J. S. Hawong, C. H. Lin, S. T. Lin, J. Rhee and R. E. Rowlands, A Hybrid Method to Determine Individual Stresses in Orthotropic Composites Using Only Measured Isochromatic Data, *Journal of Composite Material*, 29 (18) (1995) 2366-2387.
- [27] D. C. Shin, J. S. Hawong, H. J. Lee, J. H. Nam and O. S. Kwon, Application of Transparent Photoelastic Experimental Hybrid Method to the Fracture Mechanics of Isotropic Material, *Transactions of the Korean Society of Mechanical Engineers (A)*, 22 (5) 834-842.
- [28] D. C. Shin, J. S. Hawong, J. H. Nam, H. J. Lee and O. S. Kwon, Application of Transparent Photoelastic Experimental Hybrid Method for the Fracture Mechanics of Orthotropic Material, *Transactions of the Korean Society of Mechanical Engineers (A)*, 22 (6) (1998) 1036-1044.
- [29] J. S. Hawong, D. C. Shin and H. J. Lee, Photoelastic Experimental Hybrid Method for Fracture Mechanics of Anisotropic Materials, *Experimental Mechanics*, 41 (1) (2001) 92-99.
- [30] D. C. Shin, J.-S. Hawong and J.-H. Sung, Development of Dynamic Photoelastic Experimental Hybrid Method for Propagating Cracks in Orthotropic Material, *Transactions of Korean Society of Mechanical Engineers A*, 27 (8) (2003) 1273-1280.
- [31] D. C. Shin, J.-S. Hawong and S.-S. Nam, Application of the static Photoelastic Experimental Hybrid Method of the Crack Propagating Criterion for Isotropic Materials, *Transactions of Korean Society of Mechanical Engineers (A)*, 28 (8) (2004) 1229-1236.
- [32] J. S. Hawong, J. H. Nam, S. L. Han and S. H. Park, Contact stress of O-ring under uniform squeeze rate by photoelastic experimental hybrid method, *Journal of Mechanical Science and Technology*, 22 (2008) 2337-2349.
- [33] J. S. Hawong, J. H. Nam, S. L. Han, O. S. Kwon and S. H. Park, A Study on the Analysis of O-ring under Uniform Squeeze Rate and Internal Pressure by Photoelastic Experimental Hybrid Method, *Journal of Mechanical Science and Technology*, 23 (2009) 2330-2340.
- [34] J. S. Hawong, J. H. Nam, S. L. Han, O. S. Kwon and G. Kwon, A Study on the Development of a Loading Device Using a Photoelastic Stress Freezing Method for the Analysis of O-ring Stress, *Journal of Mechanical Science and Technology*, 24 (2010) 693-701.
- [35] N. I. Muskhelishvili, *Some Basic Problems of Mathematical Theory of Elasticity*, 4<sup>th</sup> Edition, P. Noordhoff Ltd., Groningen Netherlands, (1963).
- [36] A. C. Ugural and S. K. Fenster, *Advanced Strength and Applied Elasticity*, Elsevier, (1981) 70.
- [37] Y. M. Huang and R. E. Rowlands, Quantitative Stress Analysis Based on the Measured Trace of the Stress Tensor, *Journal of Strain Analysis, Eng. Design*, 26 (1) (1991) 55-63.
- [38] R. C. Sampson, A Stress-Optic Law for Photoelastic Analysis of Orthotropic Composites, *Exp. Mech.*, Vol. 10, (1970) 210-215.
- [39] *Introduction to Stress Analysis by the Photo Stress Method*, Tech Note TN-702, Measurement Group.
- [40] M. S. Bazaraa and C. M. Shetty, *Nonlinear Programming : theory and algorithms*, John Wiley & Sons Inc, (1979).
- [41] R. E. Peterson, *Stress Concentration Factors*, A Wiley-Interscience Publication.



**Jai-Sug Hawong** received a B.S. degree in Mechanical Engineering from Yeungnam University in 1974. Then he received his M.S. degree and Ph.D. degree from Yeungnam University in Korea in 1976 and from Kanto Gakuin University in Japan in 1990, respectively. Prof. Hawong is currently a professor at the school of Mechanical Engineering at Yeungnam University, in Gyeongsan city, Korea. He is currently serving as President of Korea Society Mechanical Engineering. Prof. Hawong's research interests include static and dynamic fracture mechanics, stress analysis, experimental mechanics for stress analysis and composite material, etc.



**Jeong-hwan Nam** received a B.S. degree in Mechanical Engineering from Yeungnam University in 1986. Then he received his M.S. and Ph.D. from Yeungnam University in Korea in 1996 and from Saitama Institute of Technology in Japan in 2005, respectively. Dr. Nam is currently a researcher at the school of Mechanical Engineering at Yeungnam University, in Gyeongsan city, Korea. Dr. Nam's research interests include mechanical design, stress analysis and experimental mechanics for stress analysis, etc.